

CSPENet: Contour-Aware and Saliency Priors Embedding Network for Infrared Small Target Detection

Jiakun Deng[†], Kexuan Li[†], Xingye Cui, Jiaxuan Li, Chang Long, Tian Pu^{*}, and Zhenming Peng^{*}, *Member, IEEE*

Abstract—Infrared small target detection (ISTD) plays a critical role in a wide range of civilian and military applications. Existing methods suffer from deficiencies in the localization of dim targets and the perception of contour information under dense clutter environments, severely limiting their detection performance. To tackle these issues, we propose a contour-aware and saliency priors embedding network (CSPENet) for ISTD. We first design a surround-convergent prior extraction module (SCPEM) that effectively captures the intrinsic characteristic of target contour pixel gradients converging toward their center. This module concurrently extracts two collaborative priors: a boosted saliency prior for accurate target localization and multi-scale structural priors for comprehensively enriching contour detail representation. Building upon this, we propose a dual-branch priors embedding architecture (DBPEA) that establishes differentiated feature fusion pathways, embedding these two priors at optimal network positions to achieve performance enhancement. Finally, we develop an attention-guided feature enhancement module (AGFEM) to refine feature representations and improve saliency estimation accuracy. Experimental results on public datasets NUDT-SIRST,IRSTD-1k, and NUA-SIRST demonstrate that our CSPENet outperforms other state-of-the-art methods in detection performance. The code is available at <https://github.com/IDIP2025/CSPENet>.

Index Terms—Multi-scale structural priors, target semantic embedding, feature fusion, infrared small target detection.

I. INTRODUCTION

INFRARED small target detection (ISTD), as one of the core technologies of all-weather optoelectronic sensing systems, has irreplaceable military and civilian value in precision guidance, strategic early warning, remote sensing monitoring, and related fields [1]. Due to the inherent limitations of the imaging process, infrared images have three problems: 1) Ultra-low pixel occupancy: Infrared targets typically cover less than 0.15% of the image size, resulting in the sparsity of the target. 2) Degraded signal-to-noise ratio (SNR): Dim targets and overwhelming background clutter contribute to

[†]These authors contributed equally to this work and should be considered co-first authors.

This work was supported by Natural Science Foundation of Sichuan Province of China (Grant No.2025ZNSFSC0522) and partially supported by National Natural Science Foundation of China (Grant No.61571096). (Corresponding authors: Zhenming Peng; Tian Pu.)

Jiakun Deng, Kexuan Li, Xingye Cui, Jiaxuan Li, Chang Long, Tian Pu and Zhenming Peng are with the School of Information and Communication Engineering and the Laboratory of Imaging Detection and Intelligent Perception, University of Electronic Science and Technology of China, Chengdu 610054, China (email: dengjiakun@std.uestc.edu.cn; kexuanli@std.uestc.edu.cn; cxy011211@163.com; 202422011409@std.uestc.edu.cn; lc243265379@gmail.com; putian@uestc.edu.cn; zmpeng@uestc.edu.cn)

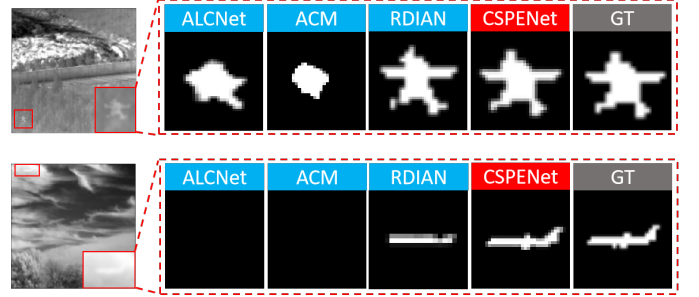


Fig. 1: Visual comparison. Segmentation results of complex-structured targets (zoomed) in dense clutter environment obtained by different methods.

a poor SNR. 3) Shape variation: Unstructured geometries resulting from variations in imaging distance, target motion, and environmental factors lead to significant changes in target appearance [81]. These problems have rendered ISTD a persistent research challenge, prompting extensive research efforts over the past few decades.

Early research efforts in ISTD predominantly relied on model-driven approaches that leveraged physical priors for target detection. Representative methods include: 1) Filter-based methods [74], [10], which assume that the background has spatial continuity and the target is abrupt singular points. 2) Human visual system (HVS)-inspired saliency detection-based methods [4], [50], which leverage contrast differences between targets and local backgrounds to detect salient targets. 3) Low-rank and sparse decomposition frameworks-based methods [72], [65], which formulate detection as a matrix decomposition problem by enforcing background low-rankness and target sparsity. While these methods offer strong interpretability and eliminate the need for large-scale training data, their performance is critically dependent on the validity of the prior assumptions. Consequently, they suffer from inherent limitations such as high parameter sensitivity and inadequate generalization in complex scenarios [81].

In recent years, the advent of a large number of annotated datasets has facilitated the development of deep learning (DL)-based ISTD methods [53], [70], [71]. These methods have outperformed traditional model-driven approaches in terms of detection accuracy and false alarm rate control, thanks to their end-to-end network architectures and backpropagation optimization mechanisms. However, current DL-based methods still encounter two significant technical challenges: 1) The inherent reliance on large-scale training data restricts

the model's ability to focus on localized patterns, leading to inaccurate target localization in dense clutter environments [61]. 2) Deep features are subject to semantic degradation since repeated convolution and pooling operations cause deep neural networks to lose low-level spatial details, thus failing to effectively preserve small target contours [41]. As shown in Fig. 1, DL-based models without embedded structural priors demonstrate inaccurate segmentation performance and frequently fail to detect targets in dense clutter scenarios.

Several existing studies have endeavored to integrate prior knowledge, such as HVS characteristics, into DL frameworks to enhance target localization and detail description capabilities [9], [68], [46]. However, the lack of consideration for the structural priors of infrared targets and the difficulty in fusing physical properties with deep representations using traditional cascaded strategies limit the improvement of model performance. Through the analysis of extensive infrared target imaging data, we observe that target contours exhibit a significant surround-convergent characteristic, as illustrated in Fig. 2. Specifically, the radiation intensity in the central region is higher than that in the surrounding edge regions, and the gradient directions of most edge pixels converge toward the target center. Leveraging this structural characteristic, we can coarsely localize dim targets, thereby effectively suppressing false alarms in complex scenes. Furthermore, the surround-contour structural priors enable finer-grained representation of the target's edge details.

In this paper, we propose a contour-aware and saliency priors embedding network (CSPENet) for ISTD, which effectively addresses the limitations of existing methods in target localization and contour detail representation by explicitly perceiving surround-convergence priors from target contours. Specifically, we design a surround-convergent prior extraction module (SCPEM), which employs multidirectional gradient magnitude calculation blocks (MGMCBs) to extract two collaborative convergent prior (CP) components: 1) CP1, a boosted saliency structure prior for precise target localization, and 2) CP2, multi-scale surround-convergent priors encoding to enhance contour hierarchical details. These components are differentially embedded into the deep network via a dual-branch priors embedding architecture (DBPEA): CP1 enhances initial target perception by jointly encoding with the input image, while CP2 dynamically interact with deep semantic features through a cross-hierarchical knowledge-infused module (CHKIM), thereby mitigating the degradation of contour details. Finally, an attention-guided feature enhancement module (AGFEM) adaptively fuses multi-layer features, enabling robust detection of weak and irregularly shaped targets. Subsequent experiments have demonstrated that our CSPENet achieves superior detection results on multiple datasets compared to other state-of-the-art (SOTA) algorithms.

In summary, our work makes four main contributions.

1) We propose CSPENet, a novel ISTD framework that embeds contour-aware and saliency priors for infrared targets into an end-to-end detection frameworks. This approach enhances the model's performance in precise target localization and detailed contour preservation under dense and cluttered

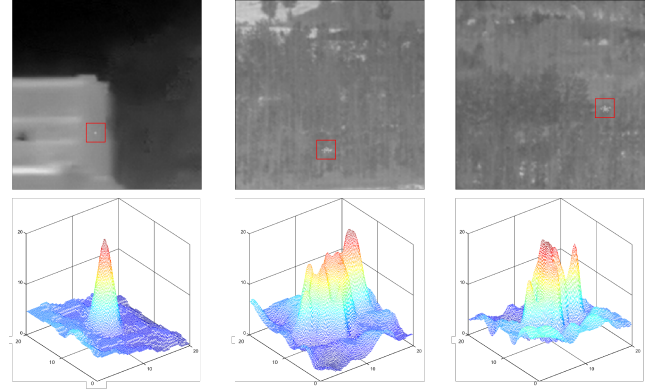


Fig. 2: Infrared small target image (upper) and its corresponding 3D local structural characterization visualization (lower).

environments.

2) We develop a structure prior extractor SCPEM to generate two collaborative priors – a boosted saliency map CP1 for precise spatial localization and multi-scale CP2 for contour detail preservation – effectively capturing both target saliency and structural characteristics.

3) We propose DBPEA to effectively embed CP components through dual pathways: CP1 directly encodes with input imagery to boost initial localization and spatial awareness, while CHKIM adaptively merges CP2 with deep features to restore semantic details and maintain structural integrity.

4) We construct AGFEM to dynamically optimize multi-layer features through attention mechanisms, significantly boosting detection performance for challenging weak or irregular targets.

II. RELATED WORK

A. Infrared Small Target Detection

1) *Model-Driven Methods*: Existing model-driven ISTD methods can be categorized into three groups: filter-based methods, HVS-based methods, and low-rank sparse decomposition-based methods. i) Filter-based methods (e.g., Top-hat [2], Max-Median [10], and 2-D adaptive TDLMS filters [39]) alongside Gaussian-derived techniques (Laplacian of Gaussian [22], Difference of Gaussian [49]) operate under the background consistency assumption, where targets disrupt local gray-level uniformity [62]. Recent advancements have mitigated limitations such as background clutter [38], [79]. ii) HVS-based methods leverage local contrast mechanisms, evolving from the foundational LCM [4] to improved variants like RLCM [14], TLLCM [15], and ADMD [33]. Recent advancements include DL-enhanced frameworks such as LELCM [63]. iii) Low-rank sparse decomposition methods, initiated by IPI [13], separate sparse targets from low-rank backgrounds through tensor modeling approaches like PSTNN [72] and tensor train/ring decomposition [51], as well as optimization improvements incorporating spatial-temporal regularization [65]. However, due to their reliance on hand-crafted shallow features, these methods often suffer from high parameter sensitivity and limited generalization capabilities in complex scenarios.

2) *Deep Learning Methods*: In recent years, DL-based methods, leveraging their adaptive feature extraction, have gradually become the dominant research paradigm in this field.

Early works were mostly based on U-Net and its variants, such as ACM [8], DNANet [26], UIUNet [58], and AMFU-net [6]. Recently, Zhang et al. [73] proposed MDIGCNet, which introduced the integrated differential convolution (IDConv) module based on the U-Net architecture to extract richer image features. Zang et al. [71] designed a dense pixel contrastive learning module aiming at capturing more features of targets with similar sizes. To break through the limitations of local receptive fields, researchers have explored the collaborative modeling mechanism of Vision Transformers (ViT) and convolutional neural networks (CNNs). Yuan et al. [70] developed SCTransNet to achieve cross-scale semantic association through a spatial channel cross-attention module. Wu et al. [57] designed MTU-Net to capture complementary global context and local detail features through a hybrid encoder of ViT and CNN. Zhu et al. [85] proposed GSTUnet that employs an edge-guided attention mechanism to selectively enhance the response in target regions. Wu et al. [53] proposed STASPPNet to optimize multi-scale feature representation using Swin Transformer with serial dilated convolutions.

Despite the significant improvement in detection performance demonstrated by DL methods, pure DL models are prone to overfitting and cross-scene generalization bottlenecks due to the high cost of infrared data annotation and inherent noise interference [61]. To address this problem, researchers have attempted to jointly design classical model-driven frameworks with DL networks. For example, the mathematical modeling of traditional filters has been transformed into learnable convolutional kernel constraints, with frequency-domain priors guiding feature extraction directions [9], [68]. Additionally, the optimization objectives of low-rank sparse decomposition have been embedded into the loss function to construct regularization constraint modules based on matrix recovery theory, suppressing redundant background components [52], [25]. However, existing methods mostly adopt loose, auxiliary combination strategies, such as simply concatenating the preprocessed results from traditional algorithms with CNN features or stacking shallow physical constraints in the loss function, failing to achieve deep integration between model-driven mechanisms and DL architectures.

B. Prior-Embedded Deep Detectors

In the field of target detection, the collaborative reasoning mechanism embedding prior knowledge into DL-based models has become a research focus in recent years. Compared with the conventional DL detection paradigm, the embedding of structured prior information introduces interpretable cognitive mechanisms for deep neural networks, effectively enhancing model robustness against occlusion, small targets, and complex scenes [60]. Existing research mainly explores three dimensions: multimodal knowledge representation, spatial relationship modeling, and scene constraint optimization. In terms of knowledge representation, Fang et al. [12] constructed an interaction mechanism between knowledge graphs and visual

features to significantly improve target recall rates through a hierarchical knowledge infusion strategy. Jiang et al. [21] designed a routing module that combines multiple types of prior knowledge to introduce semantic relationships into visual features. Xu et al. [59] innovatively proposed the spatially-aware graph convolutional network (SGRN) to jointly encode target semantics and spatial relationships. Yang et al. [64] established a knowledge-aware target detection framework to effectively solve contextual modeling challenges in large-scale detection tasks. Cheng et al. [5] built a context-aware detection framework from the perspective of scene semantic constraints to use the relationships between scenes and objects as specific prior knowledge to improve detection accuracy. Mo et al. [32] integrated geometric constraints and object co-occurrence prior knowledge to design a graph reasoning module that significantly enhances the model's deductive reasoning ability for complex target relationships.

In the ISTD field, the inherent feature sparsity of small targets [66], [44] and the limited scale of training samples make conventional DL-based models fall into the dilemma of insufficient representation learning, weakening their capability of distinguishing targets and complex background interferences. To address this issue, researchers have attempted to embed prior knowledge into DL frameworks. For example, ALCNet [9] and the MLCL [68] module embed the multi-scale patch-based contrast measure (MPCM) algorithm into the skip connections of DL networks through dilated convolution modules. Wang et al. [46] proposed a local contrast perception mechanism that jointly optimizes target enhancement and background suppression using region saliency priors. Zhao et al. [82] infused the high-frequency directional features of infrared small targets as domain-specific prior knowledge into neural networks to alleviate the limitations of small target appearance representation. ISNet [75] designed an edge-aware module based on Taylor finite difference to enhance shape prior modeling capabilities. DMEF-net [31] integrated radiance distribution and motion characteristic priors to design a multi-physical feature compensation mechanism to mitigate the data sparsity contradiction. However, existing methods struggle to effectively extract structural priors from infrared targets and fail to adequately integrate their physical attributes with deep learning representations. This leads to an inherent trade-off between target localization accuracy and detailed structural description, ultimately limiting further improvements in detection performance.

III. METHODOLOGY

A. Overall Architecture

As illustrated in Fig. 3, the CSPENet framework consists of three components: SCPEM, DBPEA, and feature enhancement module (FEM). SCPEM extracts structural prior components from the input image, specifically generating two types of CP components: one for localization enhancement (CP1) and the other for multi-scale contour detail supplementation (CP2). Subsequently, DBPEA differentially embeds CP1 and CP2 through a dual-path architecture to enhance feature representation, effectively balancing localization accuracy and contour

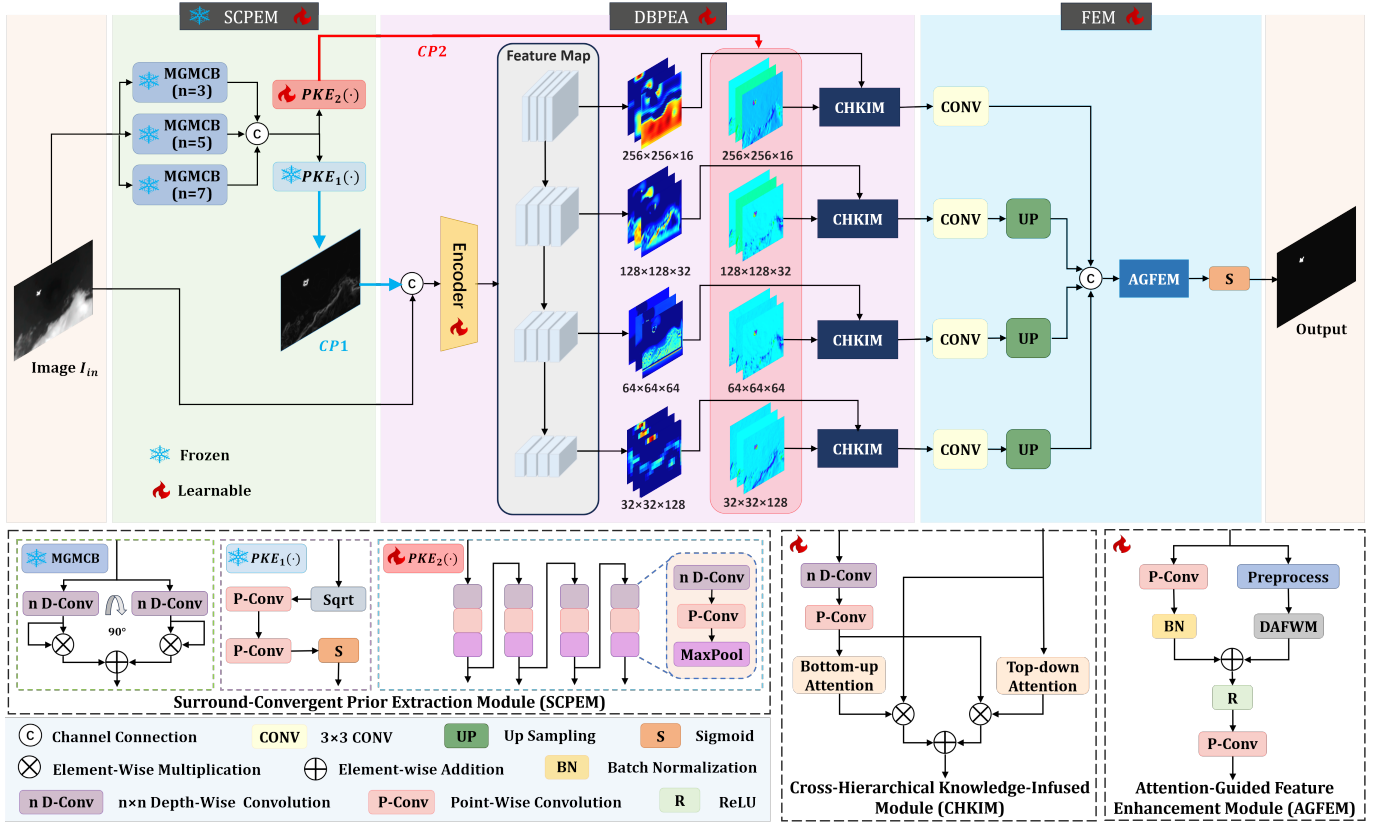


Fig. 3: The overall architecture of the proposed CSPENet for infrared small target detection. 1) SCPEM: The input image is first fed into SCPEM to obtain two types of CP components. 2) DBPEA: The two types of CP components are embedded into the deep learning network through DBPEA, where CP1 is jointly encoded with the input image via channel concatenation, and CP2 dynamically interacts with the corresponding deep semantic features through CHKIM. 3) FEM: The fused features are convolved and upsampled to a uniform scale and concatenated in the channel dimension, and then AGFEM is used to adaptively enhance the features from different layers to produce the final predicted image.

detail preservation. Finally, in FEM, features from all layers are upsampled to the same resolution and refined via AGFEM, producing a more precise target saliency map.

B. SCPEM

1) *Motivation*: The inherent thermal diffusion characteristics of infrared imaging induce distinct luminance variations between target centers and peripheral regions. Embedding such local structural priors enables ISTD systems to effectively perceive real target areas.

Existing studies, such as local binary patterns (LBP), have demonstrated effectiveness in representing invariant features for ISTD tasks [56], [69], [67]. However, these methods are limited to capturing contrast information along horizontal, vertical, and diagonal directions, making them inadequate for characterizing complex-structured targets. Recognizing that multi-directional contrast information can significantly enhance detection performance for complex-structured targets, while solely relying on contrast priors lacks detailed contour representation, we propose SCPEM. This module utilizes multi-directional Gaussian derivative kernels to capture the target's surround-convergence characteristics beyond simple contrast. The multi-directional Gaussian derivative kernels provide two key benefits: first, they enhance localization performance for complex targets by leveraging contrast information from

multiple directions; second, they capture contour details to improve target segmentation accuracy. The architecture consists of three-scale MGMCBs and two CP extraction modules.

2) *MGMCB*: The block is derived by unfolding the traditional gradient magnitude computation process into a deep network architecture. The core operation employs Gaussian derivative kernels $GD(x, y, \sigma_G, \theta_G)$ to extract oriented local structures, with the kernel defined as:

$$GD(x, y, \sigma_G, \theta_G) = -\frac{G(x, y, \sigma_G)}{\sigma_G^2} (x \cos \theta_G + y \sin \theta_G) \quad (1)$$

where $G(x, y, \sigma_G) = \left(1/\sqrt{2\pi\sigma_G^2}\right) e^{-(x^2+y^2)/2\sigma_G^2}$ denotes the Gaussian kernels with scale parameter σ_G , and θ_G denotes the partial derivative direction.

The calculation of the gradient magnitude $I_M(x, y, \sigma_G, \theta_G)$ combines the responses in orthogonal directions:

$$I_M(x, y, \sigma_G, \theta_G) = (GD(x, y, \sigma_G, \theta_G) \otimes I_{in}(x, y))^2 + (GD(x, y, \sigma_G, \theta_G + \pi/2) \otimes I_{in}(x, y))^2 \quad (2)$$

where $I_{in} \in \mathbb{R}^{W \times H \times 1}$ is the input image, and \otimes denotes convolution. W and H represent the width and height of the input respectively. To effectively capture the surround-convergence characteristics of diverse targets (particularly irregular ones), we construct the MGMCB output by stacking gradient magnitude feature maps from 24 discrete orientations

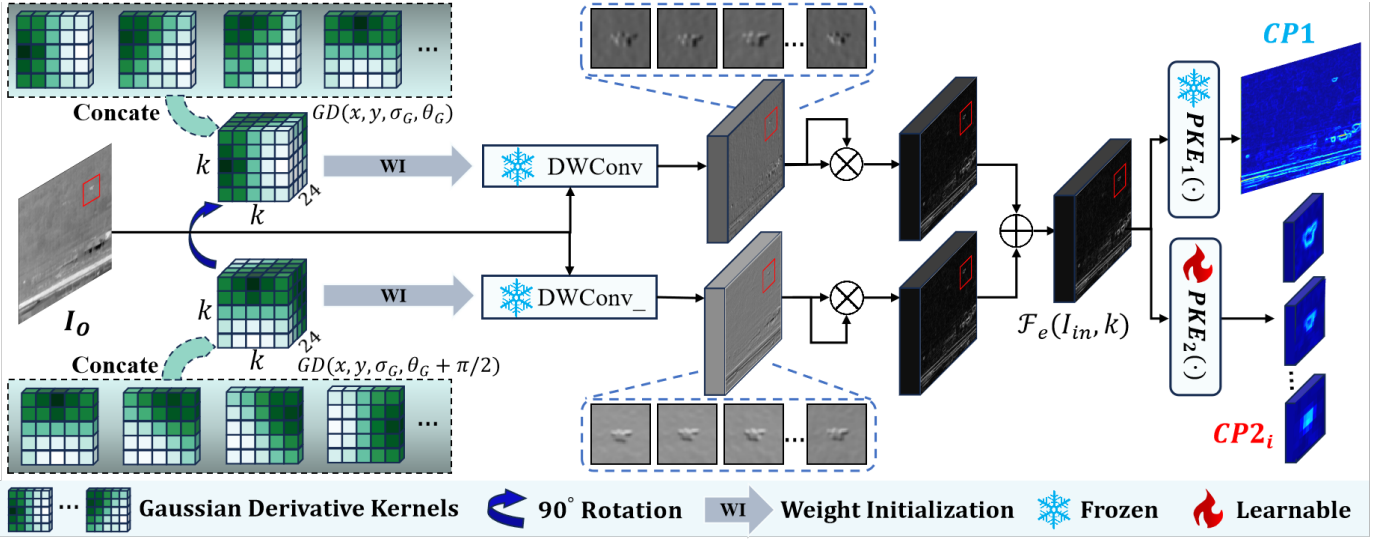


Fig. 4: The architecture of MGMCB.

$[0^\circ, 15^\circ, 30^\circ, \dots, 345^\circ]$.

For neural network implementation, we reformulate this process using depth-wise convolutions to obtain the gradient magnitude tensor $\mathcal{F}_e(I_{in}, k)$:

$$\mathcal{F}_e(I_{in}, k) = \text{DWConv}(I_{in}, k)^2 + \text{DWConv}_{-}(I_{in}, k)^2 \quad (3)$$

where both $\text{DWConv}(\cdot)$ and $\text{DWConv}_{-}(\cdot)$ represent complementary depth-wise convolutional operations that preserve the original gradient computation properties while enabling efficient network integration. k represents the size of the convolution kernel in the depth-wise convolution operation. Fig. 4 presents the architecture of MGMCB. Specifically, we construct a tensor by concatenating multiple contiguous multi-directional Gaussian derivative kernels along the channel dimension and use them to initialize the weights of one depth-wise convolution. The other depth-wise convolution adopts a 90-degree rotated version of this tensor as its initial weights. To maintain the original multidirectional gradient-convergent properties, the weights of both convolutional layers remain unchanged during training. Finally, the computed $\mathcal{F}_e(I_{in}, k)$ is used to derive the prior components CP1 and CP2.

3) *CP Extraction Modules*: Considering multi-scale object detection, the outputs of MGMCBs at three scales ($3 \times 3, 5 \times 5, 7 \times 7$) are concatenated and processed through CP extraction modules to generate two representations: a boosted prior map $CP1 \in \mathbb{R}^{W \times H \times 1}$ for precise target localization, and multi-scale hierarchical features $CP2_i \in \mathbb{R}^{(W/2^i) \times (H/2^i) \times (i+1)C}, i = 0, 1, 2, 3$ for subsequent feature embedding, where C denotes the channel dimension. This process can be represented as follows:

$$CP1 = \text{PKE}_1(\mathcal{F}_c(\mathcal{F}_e(I_{in}, 3), \mathcal{F}_e(I_{in}, 5), \mathcal{F}_e(I_{in}, 7))) \quad (4)$$

$$CP2_i = \text{PKE}_2(\mathcal{F}_c(\mathcal{F}_e(I_{in}, 3), \mathcal{F}_e(I_{in}, 5), \mathcal{F}_e(I_{in}, 7))) \quad (5)$$

where $\mathcal{F}_c(\cdot)$ denotes the feature concatenation operation, $\text{PKE}_1(\cdot)$ and $\text{PKE}_2(\cdot)$ correspond to the extraction processes of the prior components CP1 and CP2_i, respectively, the specific structures of which are shown in Fig. 3. $\text{PKE}_1(\cdot)$ employs point-wise convolution and basic operators

to generate a single-channel salient map that highlights target regions. $\text{PKE}_2(\cdot)$ utilizes a deep architecture with depth-wise separable convolutions and max-pooling modules to construct multiscale feature representations for hierarchical feature fusion. Note that the parameters in $\text{PKE}_1(\cdot)$ remain frozen (either averaging or weighted summation) to preserve full-resolution feature extraction, whereas all parameters in $\text{PKE}_2(\cdot)$ are kept learnable.

C. DBPEA

To dynamically embed CP components to the optimal positions of deep neural networks, we develop DBPEA. The key operational principles of DBPEA include:

1) *CP1 Component Embedding*: With the use of CP1's boosted spatial prior encoding target convergence patterns, we first concatenate this structurally informative component with the input image I_{in} along the channel dimension. The concatenated feature map is then processed through a U-shaped architecture, specifically an encoder-decoder subnet, to generate hierarchical features $f_i \in \mathbb{R}^{(W/2^i) \times (H/2^i) \times (i+1)C}, i = 0, 1, 2, 3$.

$$f_0, f_1, f_2, f_3 = \mathcal{F}_x(\mathcal{F}_c(I_{in}, CP1)) \quad (6)$$

where $\mathcal{F}_x(\cdot)$ signifies the mapping function learned by the U-shaped architecture. To fully extract the multi-scale feature representation of small targets, we adopt a 4-layer densely nested interactive module (DNIM) [26]. DNIM enhances feature propagation through dense connections and skip connections bridging encoder-decoder subnets, with the decoder outputs serving as the final hierarchical features.

2) *CP2 Component Embedding*: To alleviate the degradation of high-level features, we embed the knowledge-encoded CP2 components into the hierarchical features. Inspired by [27] and [19], we introduce CHKIM, which utilizes top-down and bottom-up modulation mechanisms for effective feature fusion.

The top-down modulation (shown in Fig. 5(a)) suppresses redundant feature channels through global high-level semantic information while enhancing discriminative representation. Given a low-level feature X and a high-level feature Y

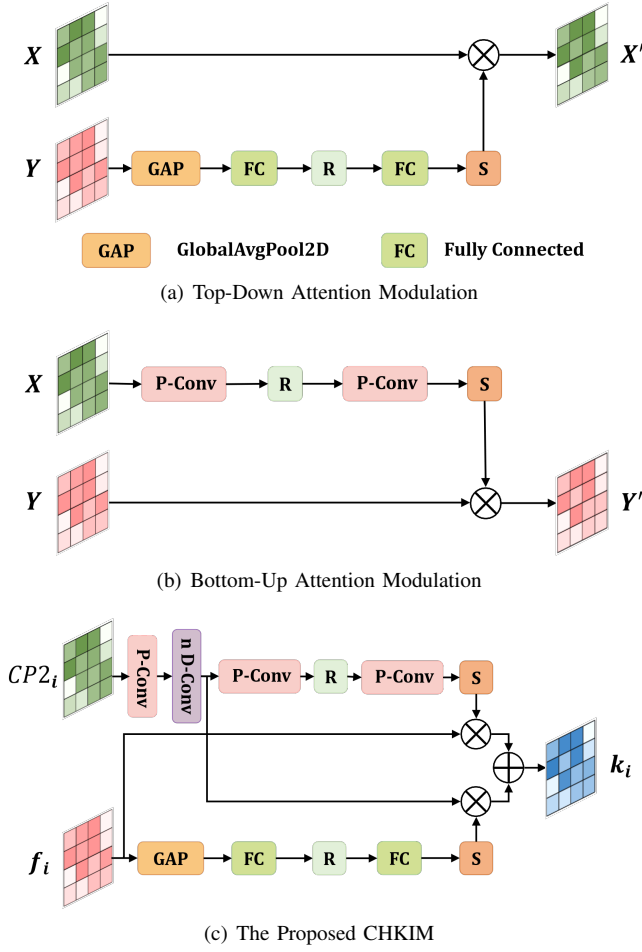


Fig. 5: Illustration of modulation modules. (a) Top-down global attentional modulation, (b) Bottom-up point-wise attentional modulation, (c) Framework diagram of the proposed CHKIM.

(both with C channels and spatial dimensions $W \times H$), the modulation process is expressed as:

$$X' = G(Y) \otimes X = \sigma(B(W_2\delta(B(W_1y)))) \otimes X \quad (7)$$

where $y = \frac{1}{W \times H} \sum_{i=1, j=1}^{W, H} Y[:, i, j]$ is the global feature context obtained through global average pooling. δ , B , σ , and \otimes denote the rectified linear unit (ReLU) [34], batch normalization (BN) [20], sigmoid function, and element-wise multiplication, respectively. $W_1 \in \mathbb{R}^{\frac{C}{r} \times C}$ and $W_2 \in \mathbb{R}^{C \times \frac{C}{r}}$ are two fully connected layers. r is the channel reduction rate.

The bottom-up modulation (shown in Fig. 5(b)) enhances the saliency of small targets in deep features through low-level details:

$$Y' = L(X) \otimes Y = \sigma(B(PWConv_2(\delta(B(PWConv_1(X))))) \otimes Y \quad (8)$$

where $PWConv(\cdot)$ denotes point-wise convolution [29]. This convolution operation is commonly used to increase or decrease the number of channels without changing the spatial dimensions of the feature map. The kernel sizes of $PWConv_1(\cdot)$ and $PWConv_2(\cdot)$ are $\frac{C}{4} \times W \times H \times C$ and $C \times W \times H \times \frac{C}{4}$, respectively. $L(X)$ has the same shape as Y and can highlight small infrared targets element-wise.

As illustrated in Fig. 5(c), CHKIM fully exploits the advantages of both modulation methods to realize effective feature interaction between shallow CP2 components and deep features f_i in an asymmetric manner:

$$k_i = G(f_i) \otimes E(CP2_i) + L(E(CP2_i)) \otimes f_i \quad (9)$$

where $k_i \in \mathbb{R}^{(W/2^i) \times (H/2^i) \times (i+1)C}$, $i = 0, 1, 2, 3$ is the fused feature, and $E(CP2_i) = PWConv(DWConv(CP2_i))$ represents the preprocessing to adjust the spatial scale and channel number of $CP2_i$. Through the asymmetric modulation of low-level details and high-level semantics, $CP2_i$ and f_i can effectively exchange high-level semantics and fine details, achieving richer encoding of semantic information and spatial details.

D. FEM

To enhance multi-scale features from multiple layers and improve the utilization rate of features, we design FEM.

First, we adopt a feature pyramid mixing mechanism to aggregate the multi-layer fused features $k_i, i = 0, 1, 2, 3$. Specifically, as shown in Fig. 3, each $k_i, i = 1, 2, 3$ is passed through a single 3×3 convolution and up-sampled to the same size, $k_i^{up} \in \mathbb{R}^{W \times H \times C}, i = 1, 2, 3$. Subsequently, the features from each layer are concatenated along the channel dimension to obtain a feature map $G = \{k_0, k_1^{up}, k_2^{up}, k_3^{up}\} \in \mathbb{R}^{W \times H \times 4C}$ with global robustness.

Subsequently, to prevent network degradation, we develop AGFEM to enhance feature representation capabilities through a residual structure, as shown in Fig. 6. Within the feature enhancement backbone, the feature map G is firstly preprocessed through a 3×3 convolution and a ReLU activation to obtain $G' \in \mathbb{R}^{W \times H \times C}$. Then, the dual-attention feature weighting module (DAFWM) is designed to adaptively enhance features to obtain $G_F \in \mathbb{R}^{W \times H \times C}$. The DAFWM consists of a channel attention (CA) unit and a spatial attention (SA) unit [42]. The CA filters out high-level semantic noise that is irrelevant to the target along the channel dimension, while the SA models global context on the feature map to refine detail features. Weighting feature maps with channel and spatial attention can

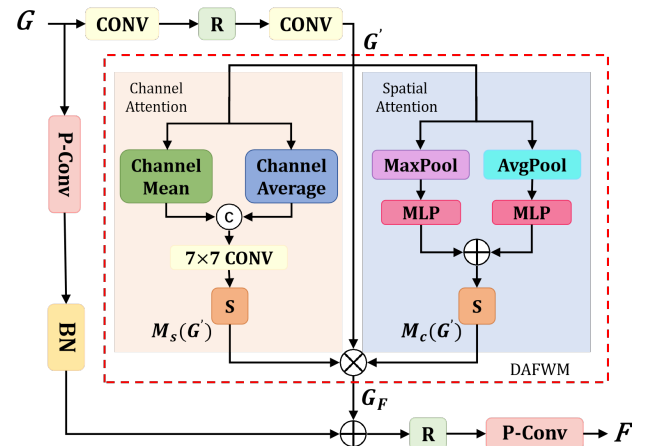


Fig. 6: The architecture of AGFEM.

enhance high-resolution detail and semantic abstraction. The DAFWM process is given by:

$$\begin{aligned} M_c(G') &= \sigma(MLP(P_{\max}(G')) + MLP(P_{\text{avg}}(G'))) \\ M_s(G') &= \sigma(\text{Conv}^{7 \times 7}(\mathcal{F}_c(CP_{\max}(G'), CP_{\text{avg}}(G')))) \\ G_F &= (M_c(G') \otimes M_s(G')) \otimes G' \end{aligned} \quad (10)$$

where $M_c(G')$ and $M_s(G')$ represent the channel attention map and spatial attention map, respectively. $P_{\max}(\cdot)$ and $P_{\text{avg}}(\cdot)$ denote the adaptive maximum pooling layer and the adaptive average pooling layer, respectively. The shared network is composed of a multi-layer perceptron (MLP) with one hidden layer. $\text{Conv}^{7 \times 7}(\cdot)$ represents the convolution operation with a 7×7 filter kernel. $CP_{\max}(\cdot)$ and $CP_{\text{avg}}(\cdot)$ denote the operations of computing the maximum and average values along the channels, respectively.

Finally, to ensure that the gradients of DAFWM do not excessively vanish or explode during backpropagation, and to preserve potential target information in the original features to avoid over-suppression of non-salient regions by the attention mechanism, we add G and G_F using a residual structure. The feature map G is first passed through a point-wise convolution and BN to match the scale with G_F , then added element-wise to the attention-weighted feature G_F , followed by ReLU activation and point-wise convolution to obtain the final feature map $F \in \mathbb{R}^{W \times H \times 1}$.

$$F = \text{PWConv}(\delta(\mathcal{B}(\text{PWConv}(G)) \oplus G_F)) \quad (11)$$

IV. EXPERIMENTS AND ANALYSIS

A. Datasets and Evaluation Metrics

1) *Datasets*: We use three publicly available datasets, including NUDT-SIRST [26], IRSTD-1k [75] and NUAA-SIRST [8]. The NUDT-SIRST dataset consists of 1327 images, with 663 images for training and 664 for testing, and images are sized at 256×256 pixels. This dataset covers five major scenes: urban, rural, ocean, heavy cloud, and highlight. The IRSTD-1K dataset contains 1001 images, with 800 for training and 201 for testing, and the image size is 512×512 pixels. It includes targets of various shapes and sizes with cluttered backgrounds. The NUAA-SIRST dataset comprises 427 images, with 213 for training and 214 for testing. The targets are faint and hidden in complex background environments, and are also subject to interference from strong light sources, sheet-like clouds, and sea surfaces.

2) *Evaluation Metrics*: We compare CSPENet with the SOTA methods using several common metrics, including intersection over union (IoU), F-measure (F_1), probability of detection (P_d), and false-alarm rate (F_a).

IoU is used to measure the degree of overlap between the predicted target region by the model and the ground-truth target region. It is described as:

$$IoU = \frac{\text{Area of Overlap}}{\text{Area of Union}} \quad (12)$$

F_1 measures precision and recall, where precision represents the ratio of correctly predicted target pixels to the total predicted target pixels, and recall represents the ratio of correctly

predicted target pixels to the total ground-truth target pixels. Its definition formula is as follows:

$$\begin{aligned} Precision &= \frac{TP}{TP + FP} \\ Recall &= \frac{TP}{TP + FN} \\ F_1 &= \frac{2 * Precision * Recall}{Precision + Recall} \end{aligned} \quad (13)$$

P_d reflects the ability to correctly detect targets, calculated as the ratio of correctly detected targets to the total number of actual targets. Its expression is given as follows:

$$P_d = \frac{T_{\text{correct}}}{T_{\text{all}}} \quad (14)$$

F_a reflects the accuracy of target detection, defined as the ratio of the number of incorrectly predicted pixels to the total number of pixels in the entire image. Its formula is expressed as:

$$F_a = \frac{P_{\text{false}}}{P_{\text{all}}} \quad (15)$$

B. Implementation Details

Our model is implemented using the PyTorch framework on a Nvidia GeForce RTX 4090 GPU. During network training, the batch size is set to 8, and the number of epochs is set to 400. We employ the Adam optimizer [23] with an initial learning rate of 5×10^{-6} , and use MultiStepLR to dynamically adjust the learning rate.

C. Comparison to SOTA Methods

To demonstrate the superiority of our method, we compare our CSPENet to several SOTA methods, including model-driven methods (MPCM [50], PSTNN [72], IPI [13]) and DL-based methods (ACM [8], ALCNet [9], AGPCNet [76], DNANet [26], UIUNet [58], RDIAN [40], RPCANet [52], MDIGCNet [73]) on the three public datasets: NUDT-SIRST [26], IRSTD-1k [75], and NUAA-SIRST [8].

1) *Quantitative Results*: The quantitative comparison of these algorithms is presented in Table I. The best results are in red, and the second best results are in blue. The symbols \uparrow and \downarrow denote metrics where higher and lower values are preferable, respectively. Specifically, although model-driven methods such as MPCM, PSTNN and IPI have relatively high P_d , they perform worse on the pixel-level metrics IoU and F_1 compared to DL-based methods, indicating insufficient detail preservation. ACM and AGPCNet demonstrate significant improvements over model-driven methods, but their performance is generally average among DL algorithms. ALCNet, despite having a relatively good P_d , only achieves an F_1 of 89.95% on NUDT-SIRST, while others exceed 90.00%. MDIGCNet achieves superior IoU scores across the three datasets, but its results in P_d are not particularly outstanding. In contrast, DNANet shows overall good performance, especially achieving the highest P_d of 98.52% on NUDT-SIRST.

The proposed CSPENet demonstrates competitive performance with relatively low computational overhead. Specifically, CSPENet achieves the preminent P_d on three datasets,

TABLE I:

COMPARISON OF DETECTION PERFORMANCE [IoU (%), F_1 (%), P_d (%), AND F_a ($\times 10^{-6}$)] AND MODEL EFFICIENCY [THE NUMBER OF PARAMETERS (M) AND THEORETICAL FLOPS (G)] OF DIFFERENT METHODS ON NUDT-SIRST, IRSTD-1K, AND NUAA-SIRST. THE BEST RESULTS ARE IN RED, AND THE SECOND BEST RESULTS ARE IN BLUE.

Methods	Params(M)	FLOPs(G)	NUDT-SIRST [26]				IRSTD-1K [75]				NUAA-SIRST [8]			
			$IoU\uparrow$	$F_1\uparrow$	$P_d\uparrow$	$F_a\downarrow$	$IoU\uparrow$	$F_1\uparrow$	$P_d\uparrow$	$F_a\downarrow$	$IoU\uparrow$	$F_1\uparrow$	$P_d\uparrow$	$F_a\downarrow$
MPCM [50]	-	-	8.18	15.12	66.14	115.96	7.33	25.89	68.73	65.12	14.87	36.27	80.06	51.43
PSTNN [72]	-	-	21.60	40.91	70.83	36.19	15.94	28.63	67.83	83.71	22.35	24.31	77.95	54.43
IPI [13]	-	-	27.60	31.82	72.28	37.28	27.60	31.82	72.28	37.28	25.67	40.18	83.27	38.92
ACM [8]	0.398	0.40	68.47	79.06	95.18	17.58	64.17	78.82	90.57	92.64	69.76	83.28	91.89	28.51
ALCNet [9]	0.378	3.74	81.24	89.95	97.57	14.37	66.02	79.06	92.58	69.45	70.21	83.46	92.78	40.34
AGPCNet [76]	12.362	43.18	87.94	90.58	97.49	7.92	66.19	79.35	89.53	26.61	75.16	85.32	93.91	45.27
DNANet [26]	4.697	14.26	92.79	96.26	98.52	4.52	65.23	79.75	92.93	40.04	74.03	87.79	95.82	43.36
UIUNet [58]	50.540	54.42	90.39	95.92	97.57	7.91	66.20	78.82	90.91	20.21	73.48	87.01	92.40	18.99
RDIAN [40]	0.022	3.72	85.70	92.18	97.88	22.81	66.02	79.69	91.57	36.44	69.81	84.88	94.42	58.58
RPCANet [52]	0.680	1.96	89.31	94.35	97.14	28.73	66.93	80.59	89.35	43.90	74.21	86.51	95.62	47.21
MDIGCNet [73]	1.505	6.557	93.41	96.03	96.67	37.28	67.09	80.44	91.25	40.38	76.23	82.37	93.65	56.84
Ours	1.440	9.49	94.18	97.00	98.52	4.92	66.79	81.10	93.27	23.53	79.83	87.41	96.96	15.18

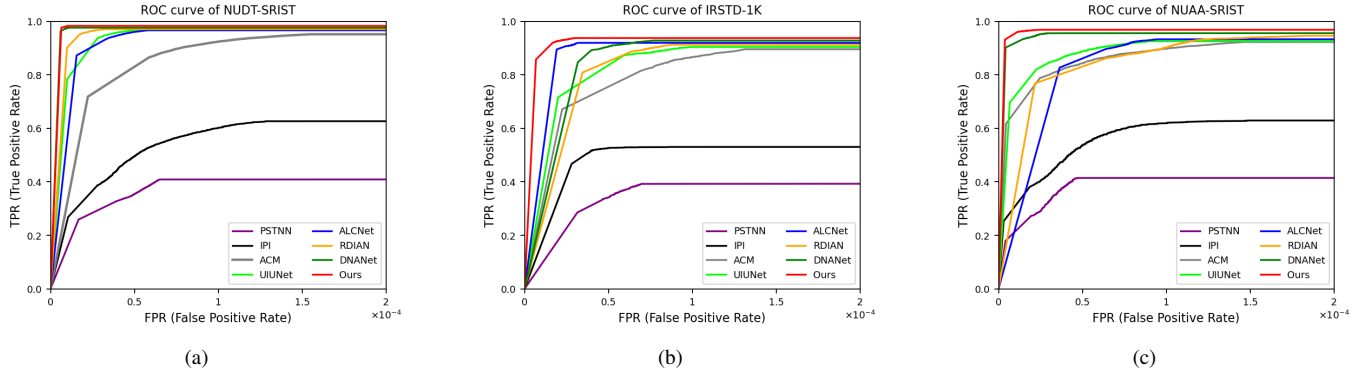


Fig. 7: ROC curves of different algorithms. (a) ROC curve of different algorithms on NUDT-SIRST. (b) ROC curve of different algorithms on IRSTD-1K. (c) ROC curve of different algorithms on NUAA-SIRST.

with especially pronounced advantages on IRSTD-1K and NUAA-SIRST, where it outperforms the second-ranking algorithms by a margin of 0.34% and 1.14%, respectively. Compared to the parameter-efficient RDIAN and ALCNet, our CSPENet demonstrates superior performance across all metrics on the three datasets. Specifically, on NUDT-SIRST, our method realizes a remarkable IoU that is 12.94% higher, an F_1 that is 7.05% elevated, a P_d that is 0.95% augmented, and a F_a that is reduced by 9.45×10^{-5} in comparison to ALCNet. In comparison with MDIGCNet, which has slightly higher parameters and computational costs, our method achieves substantial enhancements in P_d , with increases of 1.85%, 2.02%, and 3.31% on the three datasets, respectively. Other metrics are comparable to or better than those of MDIGCNet. Compared with DNANet, AGPCNet, and UIUNet, which require more parameters and higher computational costs, our CSPENet consistently realizes superior detection performance across all three datasets with less parameters. This indicates that our method balances performance and computational overhead, offering greater practicality.

Furthermore, we plot the ROC curves of various methods on NUDT-SIRST, IRSTD-1k, and NUAA-SIRST. As shown in Fig. 7, our CSPENet rapidly approaches the top-left corner across all datasets, surpassing all traditional algorithms and nearly all DL algorithms. For example, in the ROC curve of IRSTD-1K, our method reaches the corner first. Although algorithms such as DNANet and UIUNet exhibit relatively

high P_d or low F_a in Table I, they cannot compete with our method in the early stages of lower thresholds. This indicates that our method possesses exceptional detection performance with fewer false alarms.

2) *Visual Comparison:* We present the visualization outcomes of compared methods under challenging scenarios across three datasets in Fig. 8. In each figure, yellow circles indicate false positives, green boxes indicate missed detections, and the detected target areas are highlighted in red and enlarged, placed in the corner of the detection image. It is worth noting that traditional methods, exemplified by IPI and PSTNN, often generate a significant number of false positives, especially in cases where the background contains strong edges, as shown in images 000519 from NUDT-SIRST and XDU673 from IRSTD-1K. Moreover, the shapes of the targets detected by traditional methods significantly differ from the ground truth (GT), making it difficult to accurately reconstruct the actual shape of the targets, sometimes even misidentifying a single target as multiple targets. DL-based methods, such as ACM and UIUNet, also exhibit missed detections in high-illumination scenes, for instance, in images 000957 from NUDT-SIRST and XDU673 from IRSTD-1K. Additionally, these methods are prone to erroneously classifying parts of irregularly shaped targets as background, resulting in suboptimal performance in delineating target contours and an inability to accurately detect the complete shape of the target, as seen in images 000492, 000519, and 001096 from NUDT-SIRST.

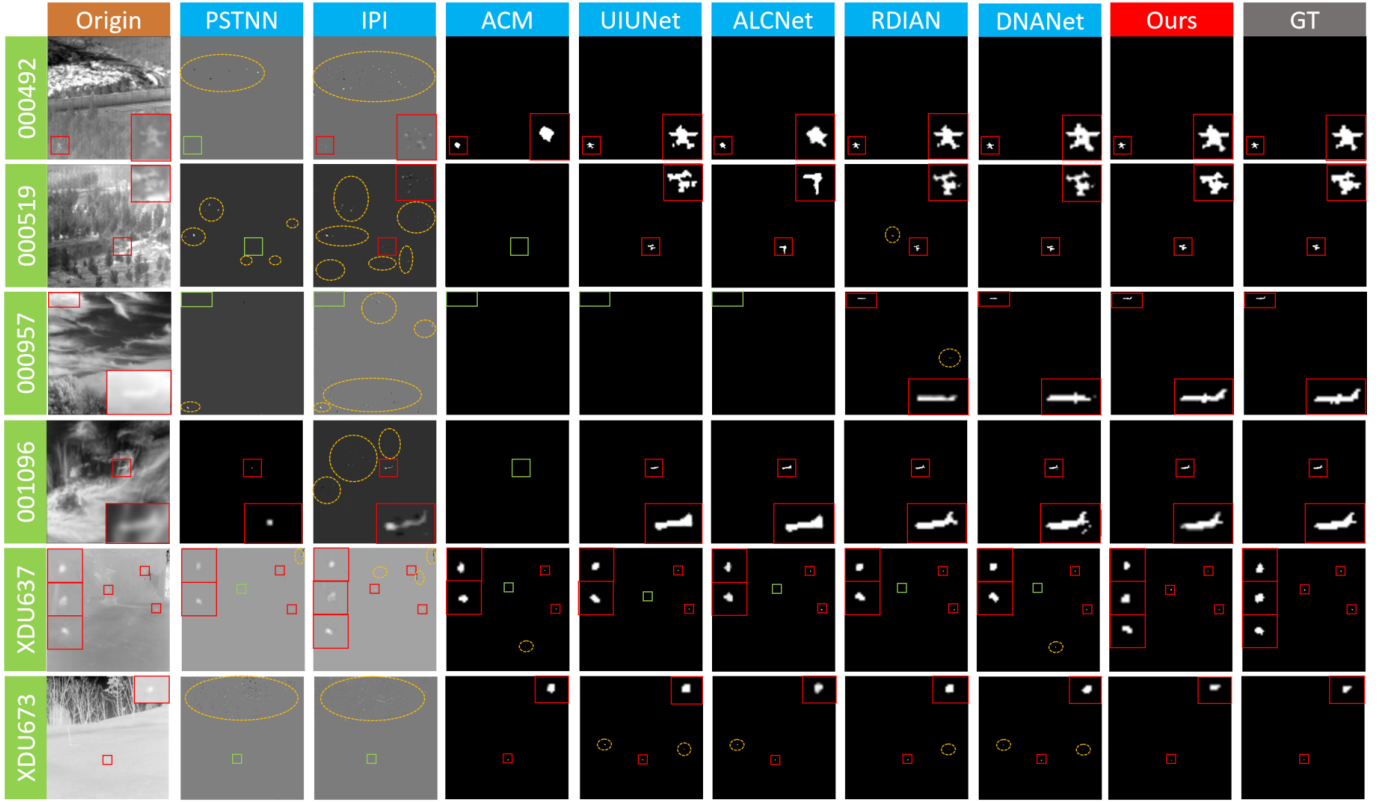


Fig. 8: Visual examples of different methods on three different datasets, with yellow circles indicating false positives and green boxes indicating missed detections. The detected target areas are highlighted in red and enlarged, placed in the corners of the detection image.

TABLE II:

ABLATION EXPERIMENTS OF QUANTITATIVE METRICS [IoU (%), F_1 (%), P_d (%), AND F_a ($\times 10^{-6}$)] WITH DIFFERENT PRIOR KNOWLEDGE EMBEDDED INTO THE BACKBONE NETWORK. THE BEST RESULTS ARE IN RED, AND THE SECOND BEST RESULTS ARE IN BLUE.

Methods	NUDT-SIRST [26]				IRSTD-1K [75]				NUAA-SIRST [8]			
	$IoU \uparrow$	$F_1 \uparrow$	$P_d \uparrow$	$F_a \uparrow$	$IoU \uparrow$	$F_1 \uparrow$	$P_d \uparrow$	$F_a \uparrow$	$IoU \uparrow$	$F_1 \uparrow$	$P_d \uparrow$	$F_a \uparrow$
backbone + Top-hat [2]	85.70	91.58	96.55	17.85	64.23	79.69	90.91	40.04	74.03	85.23	95.82	40.34
backbone + LCM [4]	87.26	92.04	97.57	18.54	64.39	79.98	91.25	42.56	74.21	85.45	96.20	45.86
backbone + MPCM [50]	85.44	92.18	96.98	23.76	64.78	79.75	91.57	48.30	74.58	85.39	95.82	47.21
backbone + IPI [13]	90.79	94.35	97.57	7.82	65.23	80.44	92.93	39.52	75.16	86.51	96.58	38.92
backbone + PSTNN [72]	92.34	93.95	97.99	6.31	65.17	80.59	92.93	36.44	74.92	87.01	96.41	36.20
backbone + SCPEM	94.18	97.00	98.52	4.92	66.79	81.10	93.27	23.53	79.83	87.41	96.96	15.18

In contrast, our CSPENet demonstrates excellent performance in multi-target and high-brightness scenarios, accurately detecting all targets with the lowest false alarm rate. In addition, the target contour is depicted more accurately. By embedding the two types of priors obtained from SCPEM via DBPEA into the network, CSPENet is able to locate small targets more accurately and extract richer contour details of target-like objects. Furthermore, the use of CHKIM for multi-hierarchical feature fusion and AGFEM for feature enhancement improves feature utilization efficiency, allowing the detection of dim targets against similar gray backgrounds, thereby reducing the occurrence of missed detections.

D. Ablation Study

To illustrate the effectiveness of the proposed CSPENet, we perform ablation studies on the key modules and evaluate their performance on the aforementioned three datasets. The structure of the rest of the network remains unchanged throughout the experiments.

1) *Effect of SCPEM*: SCPEM is designed to extract CP knowledge, generating two collaborative CP components that possess both spatial structural information and contour detail retention capabilities. To investigate the benefits brought by the prior knowledge obtained by this module, we first compare the results of using the original infrared image processed by SCPEM with those from other methods (such as Top-hat, LCM, MPCM, IPI, and PSTNN) as structural priors embedded into the backbone network through DBPEA, as shown in Table II. Among them, Top-hat performs filtering on the image, LCM and MPCM enhance the contrast of the image, and IPI and PSTNN provide sparse results of the image. It can be observed that on NUDT-SIRST, IRSTD-1K and NUAA-SIRST, the IoU , F_1 , P_d and F_a all reach the optimal values. Specifically, IoU improves by at least 1.84%, 1.56% and 4.67%, F_1 improves by at least 2.65%, 0.51% and 0.3%, P_d improves by at least 0.53%, 0.34% and 0.38%, and F_a reduces by at least 1.39×10^{-6} , 12.91×10^{-6} and 21.02×10^{-6} .

Meanwhile, we present the visualization results of different

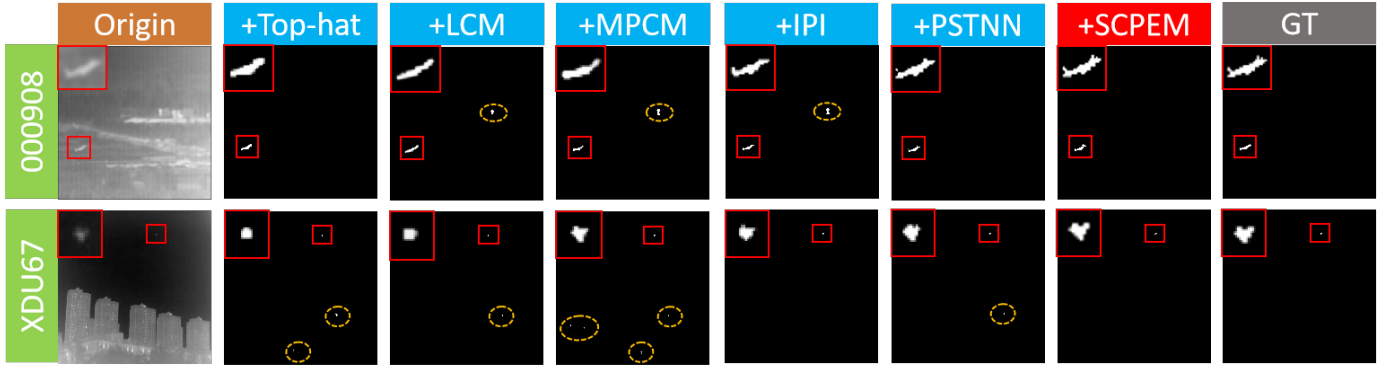


Fig. 9: Visual examples of embedding different prior knowledge into the backbone on three different datasets, with yellow circles indicating false positives. The detected target areas are highlighted in red and enlarged, placed in the corners of the detection image.

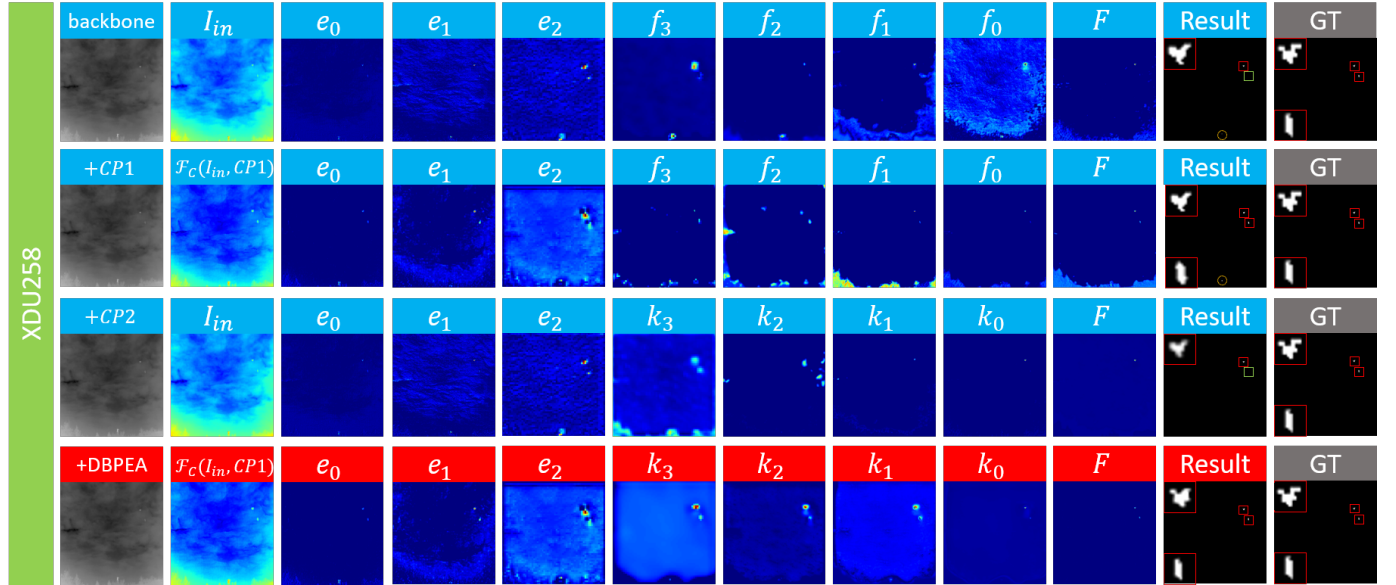


Fig. 10: Heatmap and description of detection results for an image with severe background clutter interference. The first to fourth rows of pictures represent backbone, backbone+CP1, backbone+CP2 and backbone+DBPEA, respectively.

TABLE III:

IoU (%), F_1 (%), P_d (%), AND F_a ($\times 10^{-6}$) VALUES ACHIEVED IN NUDT-SIRST, IRSTD-1K, AND NUAA-SIRST ON ABLATION EXPERIMENTS ABOUT DBPEA. THE BEST RESULTS ARE IN RED, AND THE SECOND BEST RESULTS ARE IN BLUE.

CP1	CP2	NUDT-SIRST [26]				IRSTD-1K [75]				NUAA-SIRST [8]			
		$IoU \uparrow$	$F_1 \uparrow$	$P_d \uparrow$	$F_a \downarrow$	$IoU \uparrow$	$F_1 \uparrow$	$P_d \uparrow$	$F_a \uparrow$	$IoU \uparrow$	$F_1 \uparrow$	$P_d \uparrow$	$F_a \uparrow$
×	×	90.39	95.92	97.57	7.91	65.20	78.82	90.91	40.04	73.48	87.01	92.40	43.36
✓	×	94.15	96.98	98.41	4.00	66.29	80.68	90.57	26.27	74.51	85.39	96.96	36.20
×	✓	93.34	96.55	98.41	6.60	64.39	78.94	92.26	36.91	73.16	84.50	96.20	46.01
✓	✓	94.18	97.00	98.52	4.92	66.79	81.10	93.27	23.53	79.83	87.41	96.96	15.18

methods in challenging scenarios on three datasets in Fig. 9. It can be seen that using the results of SCPEM as prior knowledge embedded into deep learning networks can accurately locate target positions, eliminate background clustering, and preserve key contour features, which proves the effectiveness of this module.

2) *Effect of DBPEA*: DBPEA is designed to collaboratively embed the CP components into the deep learning network, thereby enhancing the model's sensitivity to the location of small targets and its precise delineation of target contours. To investigate the benefits brought by this module, we compare the detection performance when using the entire architecture,

using only the first branch to embed CP1, and using only the second branch to embed CP2. Table III compares their detection performance, including IoU (%), F_1 (%), P_d (%), and F_a ($\times 10^{-6}$).

It can be observed that when CP1 or CP2 is introduced individually, the performance of the network is enhanced compared to the backbone, indicating that embedding prior information into deep learning models is effective. On the other hand, when both structures are introduced, that is, when the complete DBPEA module is utilized, the network performs even better, especially achieving the best values in IoU , F_1 , P_d , across all three datasets. This demonstrates that our

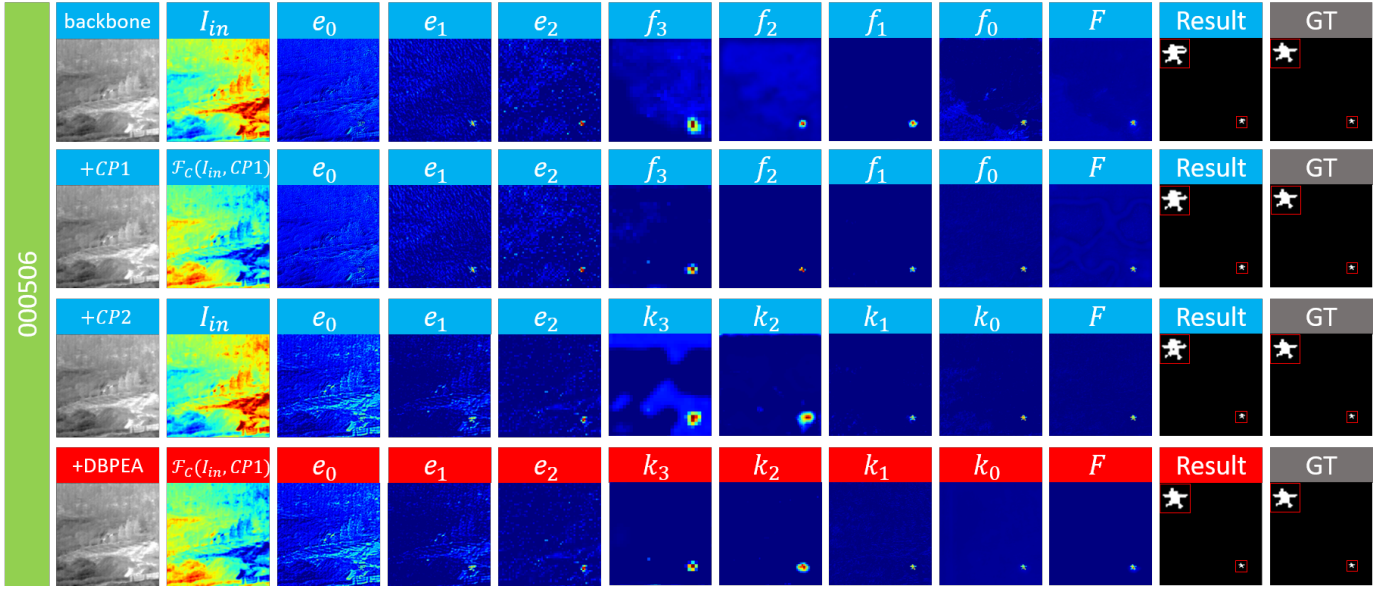


Fig. 11: Heatmap and description of detection results for an image containing an irregularly shaped target. The first to fourth rows of pictures represent backbone, backbone+CP1, backbone+CP2 and backbone+DBPEA respectively.

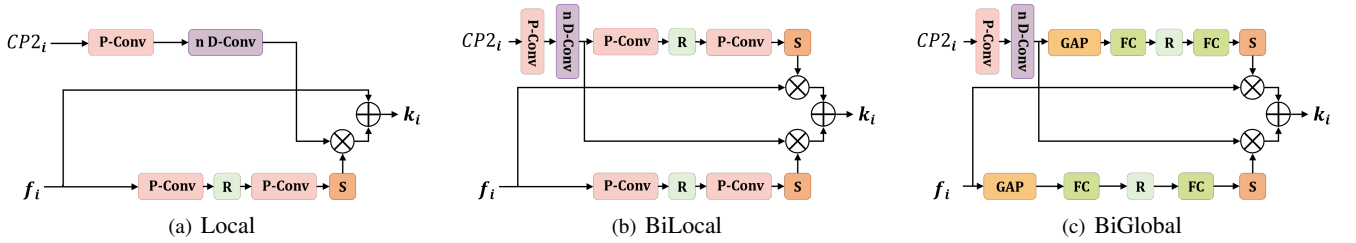


Fig. 12: Architectures for the ablation study on CHKIM. (a) Top-down modulation with point-wise channel attention module (Local). (b) Bi-directional modulation with point-wise channel attention module (BiLocal). (c) Bi-directional modulation with global channel attention module (BiGlobal).

designed DBPEA module can effectively assist the backbone network in extracting the contour details of small targets.

Additionally, to demonstrate that CP1 and CP2 can effectively extract contour information of small targets, we use images from two scenarios. As shown in Fig. 10 and Fig. 11, the first column displays the original images, I_{in} represents the heatmap of the original image, $\mathcal{F}_c(I_{in}, CP1)$ is the heatmap after fusing I_{in} with $CP1$, e_0 to e_2 denote the heatmaps at each layer of the encoding process in DNIM, f_0 to f_3 represent the heatmaps at each layer of the decoding process, k_0 to k_3 indicate the heatmaps output at each layer after fusing f_i with $CP2_i$ through CHKIM, F represents the heatmap output by AGFEM, and the last two columns are the output detection results and GT, respectively. The color intensity varies from weak to strong, indicating energy levels from low to high. It is evident that when facing multiple targets, fusing position information $CP1$ with I_{in} before feature extraction can detect dim targets against similar gray backgrounds, reducing the occurrence of missed detections and also suppress background clutter to some extent, as seen in the first and second rows in Fig. 10. Moreover, fusing f_i with $CP2_i$ can significantly reduce clutter information outside the target area, helping the

network focus on target-like regions and reduce false alarms, as illustrated in the first row and third row, columns 6 to 9 in Fig. 10. The introduction of $CP1$ and $CP2_i$ also aids in extracting detailed information from the images, better recovering the shapes of small targets, such as image in Fig. 11. The concentrated energy on the CSPENet heatmap and the detection results confirm the effectiveness of DBPEA design.

3) Effect of CHKIM: CHKIM is utilized to infuse low-level structural information into deep features to achieve feature fusion, thereby enriching the information representation and enhancing the robustness of the model. To investigate the effectiveness of this module, we compare the performance of CHKIM with three variants illustrated in Fig. 12, and the comparison results are shown in Table IV.

Firstly, we compare the one-directional top-down modulation module, i.e., Local (in Fig. 12(a)), with the two-directional modulation modules, i.e., BiLocal (in Fig. 12(b)) and BiGlobal (in Fig. 12(c)). It can be observed from Table IV that both two-directional modulation modules consistently outperformed the one-directional modulation module across all metrics. Subsequently, we compare the symmetric feature fusion modules, BiLocal and BiGlobal, with the proposed CHKIM to verify the effectiveness of asymmetric attention modulation. As shown in

TABLE IV:

THE IoU (%), F_1 (%), P_d (%), AND F_a ($\times 10^{-6}$) VALUES ACHIEVED BY THE MAIN VARIANTS OF CHKIM ON NUDT-SIRST, IRSTD-1K, AND NUAA-SIRST. THE BEST RESULTS ARE IN RED, AND THE SECOND BEST RESULTS ARE IN BLUE.

Methods	NUDT-SIRST [26]				IRSTD-1K [75]				NUAA-SIRST [8]			
	$IoU \uparrow$	$F_1 \uparrow$	$P_d \uparrow$	$F_a \uparrow$	$IoU \uparrow$	$F_1 \uparrow$	$P_d \uparrow$	$F_a \downarrow$	$IoU \uparrow$	$F_1 \uparrow$	$P_d \uparrow$	$F_a \uparrow$
Local	87.18	92.95	97.46	17.58	62.87	76.82	90.57	32.61	73.90	85.32	93.91	28.46
BiLocal	90.39	96.03	98.20	11.79	65.23	79.69	92.58	26.61	75.27	87.01	96.20	19.36
BiGlobal	91.45	95.92	98.31	7.80	64.17	79.06	92.25	23.16	76.58	86.93	96.58	18.44
CHKIM	94.18	97.00	98.52	4.92	66.79	81.10	93.27	23.53	79.83	87.41	96.96	15.18

TABLE V:

THE IoU (%), F_1 (%), P_d (%), AND F_a ($\times 10^{-6}$) VALUES ACHIEVED BY THE MAIN VARIANTS OF AGFEM ON NUDT-SIRST, IRSTD-1K, AND NUAA-SIRST. THE BEST RESULTS ARE IN RED, AND THE SECOND BEST RESULTS ARE IN BLUE.

CA	SA	Residual	NUDT-SIRST [26]				IRSTD-1K [75]				NUAA-SIRST [8]			
			$IoU \uparrow$	$F_1 \uparrow$	$P_d \uparrow$	$F_a \uparrow$	$IoU \uparrow$	$F_1 \uparrow$	$P_d \uparrow$	$F_a \uparrow$	$IoU \uparrow$	$F_1 \uparrow$	$P_d \uparrow$	$F_a \uparrow$
×	×	×	93.28	95.13	96.62	7.24	65.23	79.77	91.47	34.63	78.51	86.51	95.82	24.97
✓	✓	×	93.41	95.92	97.88	6.31	66.02	80.68	91.57	30.28	78.96	86.79	96.20	22.35
✓	×	✓	93.70	96.23	96.67	6.03	66.29	80.59	92.93	29.45	79.21	87.79	96.58	16.34
×	✓	✓	94.15	96.56	97.57	5.29	66.20	80.44	92.26	22.58	79.02	87.01	96.96	16.91
✓	✓	✓	94.18	97.00	98.52	4.92	66.79	81.10	93.27	23.53	79.83	87.41	96.96	15.18

Table IV, compared to the modulation schemes where channel attention scales are either local (BiLocal) or global (BiGlobal), the proposed CHKIM performed the best, improving IoU , F_1 , and P_d by at least 2.73%, 0.97%, and 0.21% respectively, and reducing F_a by at least 2.88×10^{-6} compared with other methods on NUDT-SIRST. Similar results are also achieved on IRSTD-1K and NUAA-SIRST. This demonstrates that CHKIM can exchange multi-layer information and produce richer feature representations.

4) *Effect of AGFEM*: AGFEM is used for adaptive feature enhancement, integrating shallow features rich in spatial information with deep features rich in semantic information to generate more robust feature maps as output. To investigate the benefits brought by this module, we compare the performance with and without AGFEM, as well as three variants of AGFEM, with the results shown in Table V.

Compared to the network without AGFEM, the addition of AGFEM led to improvements in almost all metrics across the three datasets. Specifically, IoU increases by 0.9%, 1.56%, and 1.32% on NUDT-SIRST, IRSTD-1K, and NUAA-SIRST, respectively, while F_1 increases by 0.04%, 2.24%, and 1.48%, and P_d improves by 1.9%, 1.8%, and 1.14%. Concurrently, F_a also improves. In addition, if the residual structure or spatial attention or channel attention is removed, IoU , F_1 , P_d all decrease while F_a increases compared to using the proposed AGFEM. These results confirm that AGFEM contributes positively to the overall performance.

V. CONCLUSION

This paper proposes CSPENet, a novel infrared target detection network. By embedding two collaborative priors into the network, CSPENet effectively mitigates performance degradation caused by the limitations of existing methods in terms of target localization accuracy and contour detail description. Specifically, we design SCPEM to generate two collaborative prior components: one encoding boosted saliency spatial localization constraints, and the other capturing multi-level contour detail features of the target. Building on this, DBPEA establishes differentiated feature fusion pathways, embedding these two priors at optimal positions of the network

to enhance target localization and structural detail fidelity. Additionally, we develop AGFEM to improve the feature utilization by integrating multi-scale salient features. Extensive experiments on public datasets demonstrate that our network significantly improves detection accuracy, especially in challenging scenarios involving irregular target contour, complex background noise, and low signal-to-noise ratios.

While CSPENet has shown promising results, our current validation remains limited to implementation on a popular segmentation backbone network. Our future work will aim to verify the generalizability of our designs across diverse backbone architectures. Moreover, the growing adoption of infrared images in practical applications has revealed two critical challenges requiring attention: the detection of subpixel-scale tiny targets, and the identification of objects with unstructured contour characteristics. We intend to conduct comprehensive evaluations on these datasets once they become available. In addition, with the emergence of multi-frame datasets, the development of a spatio-temporal joint modeling framework that leverages multi-frame temporal information to enhance dynamic target detection performance would be another potential direction for exploration.

REFERENCES

- [1] Lucas R Abruzzi, John-Clare Laxton, Taelor M Zarkovic, and Chris G Gill. Internal standard utilization strategies for quantitative paper spray mass spectrometry. *Journal of the American Society for Mass Spectrometry*, 2025.
- [2] Xiangzhi Bai and Fugen Zhou. Infrared small target enhancement and detection based on modified top-hat transformations. *Computers & Electrical Engineering*, 36(6):1193–1201, 2010.
- [3] Siying Cao, Jiakun Deng, Junhai Luo, Zhi Li, Junsong Hu, and Zhenming Peng. Local convergence index-based infrared small target detection against complex scenes. *Remote Sensing*, 15(5):1464, 2023.
- [4] CL Philip Chen, Hong Li, Yantao Wei, Tian Xia, and Yuan Yan Tang. A local contrast method for small infrared target detection. *IEEE transactions on geoscience and remote sensing*, 52(1):574–581, 2013.
- [5] Bei Cheng, Zhengzhou Li, Bitong Xu, Chujia Dang, and Jiaqi Deng. Target detection in remote sensing image based on object-and-scene context constrained cnn. *IEEE Geoscience and Remote Sensing Letters*, 19:1–5, 2021.
- [6] Won Young Chung, In Ho Lee, and Chan Gook Park. Lightweight infrared small target detection network using full-scale skip connection u-net. *IEEE Geoscience and Remote Sensing Letters*, 20:1–5, 2023.
- [7] Yimian Dai and Yiquan Wu. Reweighted infrared patch-tensor model with both nonlocal and local priors for single-frame small target detec-

- tion. *IEEE journal of selected topics in applied earth observations and remote sensing*, 10(8):3752–3767, 2017.
- [8] Yimian Dai, Yiquan Wu, Fei Zhou, and Kobus Barnard. Asymmetric contextual modulation for infrared small target detection. In *Proceedings of the IEEE/CVF winter conference on applications of computer vision*, pages 950–959, 2021.
 - [9] Yimian Dai, Yiquan Wu, Fei Zhou, and Kobus Barnard. Attentional local contrast networks for infrared small target detection. *IEEE transactions on geoscience and remote sensing*, 59(11):9813–9824, 2021.
 - [10] Suyog D Deshpande, Meng Hwa Er, Ronda Venkateswarlu, and Philip Chan. Max-mean and max-median filters for detection of small targets. In *Signal and Data Processing of Small Targets 1999*, volume 3809, pages 74–83. SPIE, 1999.
 - [11] Mingming Fan, Shaoqing Tian, Kai Liu, Jiaxin Zhao, and Yunsong Li. Infrared small target detection based on region proposal and cnn classifier. *Signal, Image and Video Processing*, 15(8):1927–1936, 2021.
 - [12] Yuan Fang, Kingsley Kuan, Jie Lin, Cheston Tan, and Vijay Chandrasekhar. Object detection meets knowledge graphs. In *Proceedings of the IEEE Conference on Computer Vision and Pattern Recognition (CVPR)*, International Joint Conferences on Artificial Intelligence, 2017.
 - [13] Chenqiang Gao, Deyu Meng, Yi Yang, Yongtao Wang, Xiaofang Zhou, and Alexander G Hauptmann. Infrared patch-image model for small target detection in a single image. *IEEE transactions on image processing*, 22(12):4996–5009, 2013.
 - [14] Jinhui Han, Kun Liang, Bo Zhou, Xinying Zhu, Jie Zhao, and Linlin Zhao. Infrared small target detection utilizing the multiscale relative local contrast measure. *IEEE geoscience and remote sensing letters*, 15(4):612–616, 2018.
 - [15] Jinhui Han, Saed Moradi, Iman Faramarzi, Chengyin Liu, Honghui Zhang, and Qian Zhao. A local contrast method for infrared small-target detection utilizing a tri-layer window. *IEEE Geoscience and Remote Sensing Letters*, 17(10):1822–1826, 2019.
 - [16] Jinhui Han, Saed Moradi, Iman Faramarzi, Honghui Zhang, Qian Zhao, Xiaojian Zhang, and Nan Li. Infrared small target detection based on the weighted strengthened local contrast measure. *IEEE Geoscience and Remote Sensing Letters*, 18(9):1670–1674, 2020.
 - [17] Qingyu Hou, Zhipeng Wang, Fanjiao Tan, Ye Zhao, Haoliang Zheng, and Wei Zhang. Ristdnet: Robust infrared small target detection network. *IEEE Geoscience and Remote Sensing Letters*, 19:1–5, 2021.
 - [18] Chen Hu, Yian Huang, Kexuan Li, Luping Zhang, Chang Long, Yiming Zhu, Tian Pu, and Zhenming Peng. Datransnet: dynamic attention transformer network for infrared small target detection. *IEEE Geoscience and Remote Sensing Letters*, 2025.
 - [19] Jie Hu, Li Shen, and Gang Sun. Squeeze-and-excitation networks. In *Proceedings of the IEEE conference on computer vision and pattern recognition*, pages 7132–7141, 2018.
 - [20] Sergey Ioffe and Christian Szegedy. Batch normalization: Accelerating deep network training by reducing internal covariate shift. In *International conference on machine learning*, pages 448–456. pmlr, 2015.
 - [21] Chenhan Jiang, Hang Xu, Xiaodan Liang, and Liang Lin. Hybrid knowledge routed modules for large-scale object detection. *Advances in Neural Information Processing Systems*, 31, 2018.
 - [22] Sungho Kim, Yookyung Yang, Joohyoung Lee, and Yongchan Park. Small target detection utilizing robust methods of the human visual system for 1st. *Journal of infrared, millimeter, and terahertz waves*, 30:994–1011, 2009.
 - [23] Diederik P Kingma. Adam: A method for stochastic optimization. *arXiv preprint arXiv:1412.6980*, 2014.
 - [24] Xuan Kong, Chunping Yang, Siying Cao, Chaohai Li, and Zhenming Peng. Infrared small target detection via nonconvex tensor fibered rank approximation. *IEEE Transactions on Geoscience and Remote Sensing*, 60:1–21, 2021.
 - [25] Renke Kou, Chunping Wang, Ying Yu, Zhenming Peng, Fuyu Huang, and Qiang Fu. Infrared small target tracking algorithm via segmentation network and multistrategy fusion. *IEEE Transactions on Geoscience and Remote Sensing*, 61:1–12, 2023.
 - [26] Boyang Li, Chao Xiao, Longguang Wang, Yingqian Wang, Zaiping Lin, Miao Li, Wei An, and Yulan Guo. Dense nested attention network for infrared small target detection. *IEEE Transactions on Image Processing*, 32:1745–1758, 2022.
 - [27] Hanchao Li, Pengfei Xiong, Jie An, and Lingxue Wang. Pyramid attention network for semantic segmentation. *arXiv preprint arXiv:1805.10180*, 2018.
 - [28] Ke Li, Di Wang, Zhangyuan Hu, Shaofeng Li, Weiping Ni, Lin Zhao, and Quan Wang. Fd2-net: Frequency-driven feature decomposition network for infrared-visible object detection. *arXiv preprint arXiv:2412.09258*, 2024.
 - [29] Min Lin, Qiang Chen, and Shuicheng Yan. Network in network. *arXiv preprint arXiv:1312.4400*, 2013.
 - [30] Shuai Liu, Pengfei Chen, and Marcin Woźniak. Image enhancement-based detection with small infrared targets. *Remote Sensing*, 14(13):3232, 2022.
 - [31] Tianlei Ma, Zhen Yang, Yi-Fan Song, Jing Liang, and Heshan Wang. Dmef-net: Lightweight infrared dim small target detection network for limited samples. *IEEE Transactions on Geoscience and Remote Sensing*, 61:1–15, 2023.
 - [32] Nan Mo and Ruixi Zhu. A novel transformer-based object detection method with geometric and object co-occurrence prior knowledge for remote sensing images. *IEEE Journal of Selected Topics in Applied Earth Observations and Remote Sensing*, 2024.
 - [33] Saed Moradi, Payman Moallem, and Mohamad Farzan Sabahi. Fast and robust small infrared target detection using absolute directional mean difference algorithm. *Signal Processing*, 177:107727, 2020.
 - [34] Vinod Nair and Geoffrey E Hinton. Rectified linear units improve restricted boltzmann machines. In *Proceedings of the 27th international conference on machine learning (ICML-10)*, pages 807–814, 2010.
 - [35] Jinyan Nie, Shaocheng Qu, Yantao Wei, Liming Zhang, and Lizhen Deng. An infrared small target detection method based on multiscale local homogeneity measure. *Infrared Physics & Technology*, 90:186–194, 2018.
 - [36] Meibin Qi, Liu Liu, Shuo Zhuang, Yimin Liu, Kunyuan Li, Yanfang Yang, and Xiaohong Li. Ftc-net: Fusion of transformer and cnn features for infrared small target detection. *IEEE Journal of Selected Topics in Applied Earth Observations and Remote Sensing*, 15:8613–8623, 2022.
 - [37] Xiangyang Ren, Boyang Jiao, Zhenming Peng, Renke Kou, Peng Wang, and Mingyuan Li. Msffnet: A multi-level sparse feature fusion network for infrared dim small target detection. *IEEE Journal of Selected Topics in Applied Earth Observations and Remote Sensing*, 2024.
 - [38] Yafei Shi, Yantao Wei, Huang Yao, Donghui Pan, and Guangrun Xiao. High-boost-based multiscale local contrast measure for infrared small target detection. *IEEE Geoscience and Remote Sensing Letters*, 15(1):33–37, 2017.
 - [39] Tarun Soni, James R Zeidler, and Walter H Ku. Performance evaluation of 2-d adaptive prediction filters for detection of small objects in image data. *IEEE Transactions on Image processing*, 2(3):327–340, 1993.
 - [40] Heng Sun, Junxiang Bai, Fan Yang, and Xiangzhi Bai. Receptive-field and direction induced attention network for infrared dim small target detection with a large-scale dataset irdst. *IEEE Transactions on Geoscience and Remote Sensing*, 61:1–13, 2023.
 - [41] Naftali Tishby, Fernando C Pereira, and William Bialek. The information bottleneck method. *arXiv preprint physics/0004057*, 2000.
 - [42] Fei Wang, Mengqing Jiang, Chen Qian, Shuo Yang, Cheng Li, Honggang Zhang, Xiaogang Wang, and Xiaoou Tang. Residual attention network for image classification. In *Proceedings of the IEEE conference on computer vision and pattern recognition*, pages 3156–3164, 2017.
 - [43] Huan Wang, Luping Zhou, and Lei Wang. Miss detection vs. false alarm: Adversarial learning for small object segmentation in infrared images. In *Proceedings of the IEEE/CVF international conference on computer vision*, pages 8509–8518, 2019.
 - [44] Jiaqi Wang, Kai Chen, Rui Xu, Ziwei Liu, Chen Change Loy, and Dahua Lin. Carafe: Content-aware reassembly of features. In *Proceedings of the IEEE/CVF international conference on computer vision*, pages 3007–3016, 2019.
 - [45] Kewei Wang, Shuaiyuan Du, Chengxin Liu, and Zhiguo Cao. Interior attention-aware network for infrared small target detection. *IEEE Transactions on Geoscience and Remote Sensing*, 60:1–13, 2022.
 - [46] Peichao Wang, Jiabao Wang, Yao Chen, Rui Zhang, Yang Li, and Zhuang Miao. Paying more attention to local contrast: Improving infrared small target detection performance via prior knowledge. *Engineering Applications of Artificial Intelligence*, 146:110244, 2025.
 - [47] Quan Wang, Zhendong Mao, Bin Wang, and Li Guo. Knowledge graph embedding: A survey of approaches and applications. *IEEE transactions on knowledge and data engineering*, 29(12):2724–2743, 2017.
 - [48] Xiaozhen Wang, Chengshan Han, Jiaqi Li, Ting Nie, Mingxuan Li, Xiaofeng Wang, and Liang Huang. Multiscale feature extraction u-net for infrared dim-and small-target detection. *Remote Sensing*, 16(4):643, 2024.
 - [49] Xin Wang, Guofang Lv, and Lizhong Xu. Infrared dim target detection based on visual attention. *Infrared Physics & Technology*, 55(6):513–521, 2012.
 - [50] Yantao Wei, Xinge You, and Hong Li. Multiscale patch-based contrast measure for small infrared target detection. *Pattern Recognition*, 58:216–226, 2016.

- [51] Fengyi Wu, Hang Yu, Anran Liu, Junhai Luo, and Zhenming Peng. Infrared small target detection using spatiotemporal 4-d tensor train and ring unfolding. *IEEE transactions on geoscience and remote sensing*, 61:1–22, 2023.
- [52] Fengyi Wu, Tianfang Zhang, Lei Li, Yian Huang, and Zhenming Peng. Rpcanet: Deep unfolding rpca based infrared small target detection. In *Proceedings of the IEEE/CVF Winter Conference on Applications of Computer Vision*, pages 4809–4818, 2024.
- [53] Heng Wu, Xi Huang, Chunhua He, Huapan Xiao, and Shaojuan Luo. Infrared small target detection with swin transformer-based multi-scale atrous spatial pyramid pooling network. *IEEE Transactions on Instrumentation and Measurement*, 2024.
- [54] Jialian Wu, Chunlun Zhou, Qian Zhang, Ming Yang, and Junsong Yuan. Self-mimic learning for small-scale pedestrian detection. In *Proceedings of the 28th ACM International Conference on Multimedia*, pages 2012–2020, 2020.
- [55] Lang Wu, Yong Ma, Fan Fan, Minghui Wu, and Jun Huang. A double-neighborhood gradient method for infrared small target detection. *IEEE Geoscience and Remote Sensing Letters*, 18(8):1476–1480, 2020.
- [56] Shuanglin Wu, Chao Xiao, Longguang Wang, Yingqian Wang, Jungang Yang, and Wei An. Repisd-net: Learning efficient infrared small-target detection network via structural re-parameterization. *IEEE Transactions on Geoscience and Remote Sensing*, 61:1–12, 2023.
- [57] Tianhao Wu, Boyang Li, Yihang Luo, Yingqian Wang, Chao Xiao, Ting Liu, Jungang Yang, Wei An, and Yulan Guo. Mtu-net: Multilevel transunet for space-based infrared tiny ship detection. *IEEE Transactions on Geoscience and Remote Sensing*, 61:1–15, 2023.
- [58] Xin Wu, Danfeng Hong, and Jocelyn Chanussot. Uiu-net: U-net in u-net for infrared small object detection. *IEEE Transactions on Image Processing*, 32:364–376, 2022.
- [59] Hang Xu, Chenhan Jiang, Xiaodan Liang, and Zhenguo Li. Spatial-aware graph relation network for large-scale object detection. In *Proceedings of the IEEE/CVF Conference on Computer Vision and Pattern Recognition*, pages 9298–9307, 2019.
- [60] Hang Xu, Chenhan Jiang, Xiaodan Liang, Liang Lin, and Zhenguo Li. Reasoning-rnn: Unifying adaptive global reasoning into large-scale object detection. In *Proceedings of the IEEE/CVF conference on computer vision and pattern recognition*, pages 6419–6428, 2019.
- [61] Shibiao Xu, Shuchen Zheng, Wenhao Xu, Rongtao Xu, Changwei Wang, Jiguang Zhang, Xiaoqiang Teng, Ao Li, and Li Guo. Hcf-net: Hierarchical context fusion network for infrared small object detection. In *2024 IEEE International Conference on Multimedia and Expo (ICME)*, pages 1–6. IEEE, 2024.
- [62] Yunkai Xu, Minjie Wan, Xiaojie Zhang, Jian Wu, Yili Chen, Qian Chen, and Guohua Gu. Infrared small target detection based on local contrast-weighted multidirectional derivative. *IEEE Transactions on Geoscience and Remote Sensing*, 61:1–16, 2023.
- [63] Dongning Yang, Haopeng Zhang, Ying Li, and Zhiguo Jiang. Label evolution based on local contrast measure for single-point supervised infrared small target detection. *IEEE Transactions on Geoscience and Remote Sensing*, 2024.
- [64] Zixuan Yang, Xiujuan Chai, Ruiping Wang, Weijun Guo, Weixuan Wang, Li Pu, and Xilin Chen. Prior knowledge guided small object detection on high-resolution images. In *2019 IEEE International Conference on Image Processing (ICIP)*, pages 86–90. IEEE, 2019.
- [65] Haiyang Yi, Chunping Yang, Ruochen Qie, Jingwen Liao, Fengyi Wu, Tian Pu, and Zhenming Peng. Spatial-temporal tensor ring norm regularization for infrared small target detection. *IEEE Geoscience and Remote Sensing Letters*, 20:1–5, 2023.
- [66] Xinyi Ying, Li Liu, Yingqian Wang, Ruojing Li, Nuo Chen, Zaiping Lin, Weidong Sheng, and Shilin Zhou. Mapping degeneration meets label evolution: Learning infrared small target detection with single point supervision. In *Proceedings of the IEEE/CVF Conference on Computer Vision and Pattern Recognition*, pages 15528–15538, 2023.
- [67] Xinyi Ying, Yingqian Wang, Longguang Wang, Weidong Sheng, Li Liu, Zaiping Lin, and Shilin Zhou. Local motion and contrast priors driven deep network for infrared small target superresolution. *IEEE Journal of Selected Topics in Applied Earth Observations and Remote Sensing*, 15:5480–5495, 2022.
- [68] Chuang Yu, Yunpeng Liu, Shuhang Wu, Zhuhua Hu, Xin Xia, Deyan Lan, and Xin Liu. Infrared small target detection based on multiscale local contrast learning networks. *Infrared Physics & Technology*, 123:104107, 2022.
- [69] Zitong Yu, Chenxu Zhao, Zezheng Wang, Yunxiao Qin, Zhuo Su, Xiaobai Li, Feng Zhou, and Guoying Zhao. Searching central difference convolutional networks for face anti-spoofing. In *Proceedings of the IEEE/CVF conference on computer vision and pattern recognition*, pages 5295–5305, 2020.
- [70] Shuai Yuan, Hanlin Qin, Xiang Yan, Naveed Akhtar, and Ajmal Mian. Sctransnet: Spatial-channel cross transformer network for infrared small target detection. *IEEE Transactions on Geoscience and Remote Sensing*, 2024.
- [71] Dongyuan Zang, Weihua Su, Bonan Zhang, and Huixin Liu. Dcanet: Dense convolutional attention network for infrared small target detection. *Measurement*, 240:115595, 2025.
- [72] Landan Zhang and Zhenming Peng. Infrared small target detection based on partial sum of the tensor nuclear norm. *Remote Sensing*, 11(4):382, 2019.
- [73] Luping Zhang, Junhai Luo, Yian Huang, Fengyi Wu, Xingye Cui, and Zhenming Peng. Mdigncnet: Multi-directional information-guided contextual network for infrared small target detection. *IEEE Journal of Selected Topics in Applied Earth Observations and Remote Sensing*, 2024.
- [74] Mingjin Zhang, Qian Xu, Yuchun Wang, Xi Li, and Haojuan Yuan. Mirsam: multimodal vision-language segment anything model for infrared small target detection. *Visual Intelligence*, 3(1):1–13, 2025.
- [75] Mingjin Zhang, Rui Zhang, Yuxiang Yang, Haichen Bai, Jing Zhang, and Jie Guo. Isnet: Shape matters for infrared small target detection. In *Proceedings of the IEEE/CVF Conference on Computer Vision and Pattern Recognition*, pages 877–886, 2022.
- [76] Tianfang Zhang, Siying Cao, Tian Pu, and Zhenming Peng. Agpcnet: Attention-guided pyramid context networks for infrared small target detection. *arXiv preprint arXiv:2111.03580*, 2021.
- [77] Tianfang Zhang, Lei Li, Siying Cao, Tian Pu, and Zhenming Peng. Attention-guided pyramid context networks for detecting infrared small target under complex background. *IEEE Transactions on Aerospace and Electronic Systems*, 59(4):4250–4261, 2023.
- [78] Tong Zhang, Yin Zhuang, Guanqun Wang, He Chen, Hao Wang, Lianlin Li, and Jun Li. Controllable generative knowledge driven few-shot object detection from optical remote sensing imagery. *IEEE Transactions on Geoscience and Remote Sensing*, 2025.
- [79] Xiangyue Zhang, Jingyu Ru, and Chengdong Wu. Infrared small target detection based on gradient correlation filtering and contrast measurement. *IEEE Transactions on Geoscience and Remote Sensing*, 61:1–12, 2023.
- [80] Yuting Zhang, Zhengzhou Li, Abubakar Siddique, Abdullah Azeem, Wenhao Chen, and Dong Cao. Infrared small target detection based on interpretation weighted sparse method. *IEEE Transactions on Geoscience and Remote Sensing*, 2025.
- [81] Zaiyan Zhang, Yangyang Zhuang, Weidong Song, Jiachen Wu, Xin Ye, Hongyue Zhang, Yanli Xu, and Guoli Shi. Ist-cracknet: Hybrid cnn-transformer models focusing on fine-grained segmentation of multi-scale pavement cracks. *Measurement*, page 117215, 2025.
- [82] Jinmiao Zhao, Zelin Shi, Chuang Yu, and Yunpeng Liu. Multi-scale direction-aware network for infrared small target detection. *arXiv preprint arXiv:2406.02037*, 2024.
- [83] Mingxin Zhao, Li Cheng, Xu Yang, Peng Feng, Liyuan Liu, and Nanjian Wu. Tbc-net: A real-time detector for infrared small target detection using semantic constraint. *arXiv preprint arXiv:2001.05852*, 2019.
- [84] Dali Zhou and Xiaodong Wang. Research on high robust infrared small target detection method in complex background. *IEEE Geoscience and Remote Sensing Letters*, 20:1–5, 2023.
- [85] Yiming Zhu, Yong Ma, Fan Fan, Jun Huang, Kangle Wu, and Ge Wang. Towards accurate infrared small target detection via edge-aware gated transformer. *IEEE Journal of Selected Topics in Applied Earth Observations and Remote Sensing*, 2024.



Jiakun Deng received the M.S. degree in Optical Engineering from the School of Optoelectronic Science and Engineering, University of Electronic Science and Technology of China (UESTC), Chengdu, China, in 2022. He is currently pursuing the Ph.D. degree in Electronic Information with the School of Information and Communication Engineering, UESTC. His research interests include computer vision, infrared small target detection and tracking, and object recognition.



KeXuan Li received the B.S. degree from Huaqiao University, Quanzhou, China in 2023. She is currently working toward the M.E. degree in electronic information with the School of Information and Communication Engineering, University of Electronic Science and Technology of China, Chengdu, China. Her research interests include image processing, computer vision, and infrared small target detection.



Xingye Cui received the B.E. degree in communication engineering from the School of Computer Science, Jiangsu University of Science and Technology, Zhenjiang, China, in 2023. She is currently working toward the M.E. degree in electronic information with the School of Information and Communication Engineering, University of Electronic Science and Technology of China, Chengdu, China. Her research interests include image processing, computer vision, and infrared small target detection.



Jiaxuan Li graduated from Wuhan University of Technology in 2024 with a Bachelor's degree. She is currently pursuing a Master's degree at the University of Electronic Science and Technology of China in Chengdu, China. Her research interests primarily focus on the fields of target recognition, image processing, and computer vision.



Chang Long received the B.E. degree from the School of Information and Communication Engineering, University of Electronic Science and Technology of China (UESTC), Chengdu, China, in 2023. He is currently working toward the M.E. degree in information and communication engineering with the School of Information and Communication Engineering, UESTC, Chengdu, China. His research interests include image processing, computer vision, and infrared small target detection.



Tian Pu graduated from Wuhan University of Technology in 2024 with a Bachelor's degree. She is currently pursuing a Master's degree at the University of Electronic Science and Technology of China in Chengdu, China. Her research interests primarily focus on the fields of target recognition, image processing, and computer vision.



Zhenming Peng (Member, IEEE) received his Ph.D. degree in geodetection and information technology from the Chengdu University of Technology, Chengdu, China, in 2001. From 2001 to 2003, he was a post-doctoral researcher with the Institute of Optics and Electronics, Chinese Academy of Sciences, Chengdu, China. He is currently a Professor with the University of Electronic Science and Technology of China, Chengdu. His research interests include image processing, machine learning, objects detection and remote sensing applications.

Prof. Peng is members of many academic organizations, such as Institute of Electrical and Electronics Engineers (IEEE), Optical Society of America (OSA), China Optical Engineering Society (COES), Chinese Association of Automation (CAA), Chinese Society of Astronautics (CSA), Chinese Institute of Electronics (CIE), and China Society of Image and Graphics (CSIG), etc.